






## Accessing the full capabilities of filter functions: Tool for detailed noise and quantum control susceptibility analysis

Ingvild Hansen <sup>1</sup>, Amanda E. Seedhouse <sup>1</sup>, Andre Saraiva <sup>1,2</sup>, Andrew S. Dzurak <sup>1,2</sup>, and Chih Hwan Yang <sup>1,2</sup>

<sup>1</sup>*School of Electrical Engineering and Telecommunications, The University of New South Wales, Sydney, New South Wales 2052, Australia*

<sup>2</sup>*Diraq, Sydney, New South Wales, Australia*



(Received 3 March 2023; accepted 7 July 2023; published 24 July 2023)

The filter function formalism from quantum control theory is typically used to determine the noise susceptibility of pulse sequences by looking at the overlap between the filter function of the sequence and the noise power spectral density. Importantly, the square modulus of the filter function is used for this method. In this work we show that by using the square modulus one neglects valuable information about the system dynamics. We take advantage of the full filter function by including information about the phase of the perturbation and the resulting rotation axis. By decomposing the filter function with phase preservation before taking the modulus, we are able to consider the contributions to  $x$ ,  $y$ , and  $z$  rotations separately. Continuously driven systems provide noise protection in the form of dynamical decoupling by canceling low-frequency noise; however, generating control pulses synchronously with an arbitrary driving field is not trivial. Using the decomposed filter function we look at the controllability of a system under arbitrary driving fields, as well as the noise susceptibility, and also relate the filter function to the geometric formalism.

DOI: [10.1103/PhysRevA.108.012426](https://doi.org/10.1103/PhysRevA.108.012426)

### I. INTRODUCTION

One of the biggest hurdles in realizing a large-scale quantum computer is mitigating decoherence caused by noise in the qubit environment. Qubits are notoriously sensitive to noise originating from the material stack, control instruments, etc. [1,2]. There are many means to reduce the effect of noise sources in qubit devices, such as isotropic purification of the host material [3] and feedback protocols [4–6]; however, the residual noise still limits qubit performance.

Different qubit modalities are plagued by different noise frequency distributions. Qubits in the solid state, for example, are typically dominated by  $1/f$  noise [2,7]. One method to tackle this type of noise is through continuous driving. Driven two-level systems, often referred to as microwave dressed systems [8–10], are continuously decoupled from environmental noise. Moreover, by tailoring the amplitude modulation of the driving field one can achieve higher-order noise protection [11]. This control strategy is compatible with global control [10,12], which is promising for scalability. Single-qubit control is implemented by applying an additional local control pulse, to dynamically control the individual qubit frequency, on top of the continuous global microwave drive. However, working out the required wave form of the local control pulses to be applied synchronously with the continuous driving field is not trivial.

Here we develop a generalized method to find the wave form of the local control pulses required for two-axis control of a two-level system driven by an arbitrary global driving field. The global driving field decouples the system from low-frequency noise, whereas the local control pulses allow for single-qubit addressability. We find the local control pulses by decomposing the filter function calculated from Magnus

expansion series and including phase information about the perturbation term. We show how this is related to the geometric formalism [13,14] and how the accumulated effect of noise or control pulses is expressed in a three-dimensional (3D) space representation. This work expands on similar methods [15–18] that were previously developed for noise analysis, with tools for a more general analysis of the control of driven systems. More specifically, the developed methods are important in the context of driven qubit control protocols [10,11,19] in order to understand the origin of the local control pulses and the noise-canceling properties of the global driving fields.

This work is applicable to any quantum-information-processing platform including quantum dots, donors, superconducting platforms, ion traps, etc., where the circuit model is typically used to model quantum computation [20]. We stress that the directional information extracted in this work does not necessarily have any physical meaning for filter function applications other than qubit dynamics. We also note that the perturbation term in this work can take fixed frequency and phase values.

### II. CALCULATION OF THE COMPLEX FILTER FUNCTION

A driven qubit subject to a single quasistatic noise source can be described by the rotating frame Hamiltonian

$$\begin{aligned} H_r(t) &= H_{\text{drive}}(t) + \delta H \\ &= \Omega_{\text{RI}}(t)\sigma_x + \Omega_{\text{RQ}}(t)\sigma_y + \delta\beta\sigma_z. \end{aligned} \quad (1)$$

Here,  $\Omega_{\text{RI/Q}}(t)$  describes the envelope of arbitrary driving fields along perpendicular axes,  $\sigma_n$  ( $n = x, y, \text{ and } z$ ) are the Pauli matrices, and  $\delta\beta$  is a small perturbation term. We will

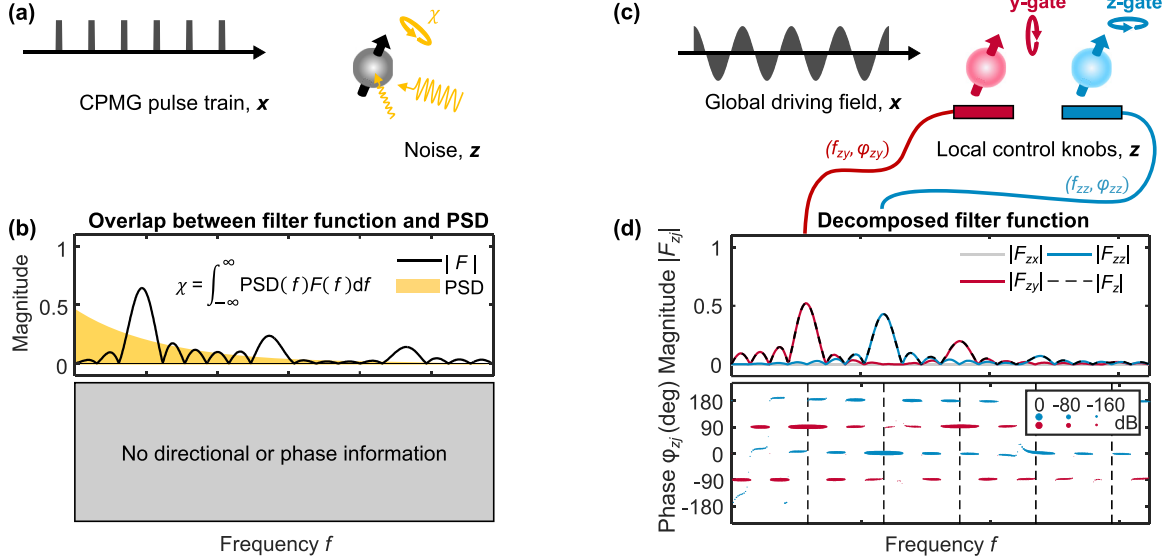


FIG. 1. Common use of filter function for noise susceptibility and improved method for control susceptibility. (a) A CPMG pulse train produces a filter function (b) which overlaps with the power spectral density results in some noise rotation magnitude  $\chi$ . (c) For a driven system the decomposed filter function gives access to the rotation axis and information about the susceptibility as a function of perturbation frequency and phase (d), which can be used as two-axis control parameters to be applied synchronously with the global field through local control knobs.

from now on assume a driving field along  $x$  and a perturbation along  $z$  ( $\sigma_i = \sigma_z$ ). However, we note that the driving axis and the perturbation axis can be arbitrarily chosen. By choosing the perturbation axis along  $z$ , it represents detuning. If we were to choose  $x$  instead ( $\sigma_i = \sigma_x$ ), it would represent a perturbation of the driving field amplitude. One can think of the perturbation as either stochastic noise or an intentionally applied control pulse with well-defined frequency and phase. This can be seen in Fig. 1, where the spin in panel (a) has a noise perturbation and the other two spins in panel (c) have control perturbations. We start out by treating  $\delta\beta$  as noise, and we come back to control later. By noise we refer to stochastic processes relevant to the system at hand causing perturbations. For silicon metal-oxide-semiconductor quantum dots, for example, magnetic noise from  $^{29}\text{Si}$  isotopes and charge noise are relevant [2].

It is useful to move into an interaction picture set by the global driving field in order to isolate the effect of the perturbation in a noise propagator,

$$\begin{aligned} H_z^{\text{int}}(t) &= \delta\beta U_{\text{drive}}^\dagger(t) \sigma_z U_{\text{drive}}(t) \\ &= \delta\beta \sum_{j=x,y,z} R_j(t) \sigma_j, \end{aligned} \quad (2)$$

where the rotation matrix is given by [15]

$$R_j(t) = \text{Tr}[U_{\text{drive}}^\dagger(t) \sigma_z U_{\text{drive}}(t) \sigma_j] / 2. \quad (3)$$

Here,  $U_{\text{drive}}$  is the time evolution operator derived from  $H_{\text{drive}}$ . By integrating  $H_z^{\text{int}}(t)$  over time, we find the accumulated effect from the perturbation in the frame of the driving field, described in first-order Magnus expansion by

$$A_{1z}(t) = \frac{1}{\delta\beta} \int_0^t H_z^{\text{int}}(t) dt. \quad (4)$$

Here,  $z$  represents the perturbation axis. Higher-order terms of the Magnus expansion can be included for a more accurate representation of the accumulated effect of the noise. The perturbation magnitude  $\delta\beta$  is, in general, limited to small values compared to the terms in  $H_{\text{drive}}$  to avoid higher-order terms. That is, we are restricted to the weak noise (or control) regime.

Equation (4) equals zero if the global driving field cancels out the effect of the perturbation to the first order. On the other hand, if the perturbation introduces rotation around  $\sigma_k$  after time  $T$ ,  $A_{1z}(T)$  is proportional to  $\sigma_k$ . Equation (4) is used in the geometric formalism in order to describe cancellation of quasistatic noise using 3D space curves [13]. Details about the connection between filter functions and the geometric formalism are discussed later.

By multiplying the integrand in Eq. (4) with a complex exponential function, we look at the effect of the perturbation at different frequencies and phases. That is, we replace the quasistatic perturbation term  $\delta\beta$  with the ac complex term  $\underline{\delta\beta}(f, t) = \hat{\delta\beta} e^{i(2\pi ft)}$ . The underline notation here refers to a phasor and the hat notation refers to the magnitude of the phasor. Hence,  $\underline{\delta\beta}(f, t)$  is a complex number containing frequency and phase information. The interaction picture Hamiltonian is now a function of time and perturbation frequency:

$$H_z^{\text{int}}(f, t) = \underline{\delta\beta}(f, t) U_{\text{drive}}^\dagger(t) \sigma_z U_{\text{drive}}(t). \quad (5)$$

This results in a generalized form of the interaction picture and after integrating over time we get what we call the first-order filter function of the driving field:

$$\underline{F}_z(f, t) = \frac{1}{\hat{\delta\beta} t} \int_0^t H_z^{\text{int}}(f, \tau) d\tau. \quad (6)$$

Here the complex exponential represents a perturbation with defined frequency  $f$  applied for a time  $t$  along axis  $z$ .

By using a phasor, we can assess the phase as well as the frequency sensitivity. Using a symmetry argument, we subtract the total time divided by 2 in the complex exponential. This effectively sets the phase of the perturbation from the center of the sequence, which simplifies the phase information for plotting and presentation purposes. The filter function is normalized with time so that the magnitude corresponds to the rotation efficiency, and by increasing the total time of the driving, the filter bandwidth becomes narrower as expected from Fourier analysis.

The filter function from Eq. (6) at any given time is a  $2 \times 2 \times N$  complex matrix, where  $N$  is the number of frequency samples. In order to look at the directional and phase information, this matrix is decomposed by taking the trace with the product of the Pauli matrices. This results in a  $3 \times N$  complex vector,

$$\underline{F}_z(f) = [F_{zx}(f), F_{zy}(f), F_{zz}(f)] \cdot [\sigma_x, \sigma_y, \sigma_z], \quad (7)$$

where the Pauli components are defined according to

$$F_{zj}(f) = \text{Tr}[\underline{F}_z(f) \cdot \sigma_j]. \quad (8)$$

For the case of single-qubit dynamics, this three-dimensional vector intuitively represents rotation in a Cartesian coordinate system. For the two-qubit case, on the other hand, the vector has 15 dimensions (e.g.,  $F_{[z \otimes I][x \otimes y]}$ ,  $F_{[z \otimes I][x \otimes I]}$ ) and arbitrary phase information for both qubits. Therefore, the directional information becomes less intuitive. The maximum magnitude of the rotation around axis  $j$  and the corresponding phase of

the perturbation for the single-qubit case can be calculated according to

$$|F_{zj}(f)| = \text{mag}[F_{zj}(f)], \quad (9)$$

$$\phi_{zj}(f) = \text{arg}[F_{zj}(f)]. \quad (10)$$

Here,  $\phi_{zj} = 0$  corresponds to a cosine wave form centered around  $T/2$ . It is also possible to calculate the rotation magnitude for the arbitrary perturbation phase (not necessarily the maximum rotation magnitude) by multiplying Eq. (6) by an arbitrary complex exponential and taking the real part before taking the trace of the product with the Pauli matrices:

$$F_{zj}(f, \phi) = \text{Tr}(\text{Re}[F_z(f) \times e^{-i\phi}] \cdot \sigma_j) = \text{Re}[F_{zj}(f) \times e^{-i\phi}]. \quad (11)$$

The method described above is a more complete way of calculating the filter function compared to the conventional one [21–28], where the squared absolute value of the Fourier transform of the time-domain filter function or switching function is used:

$$F(f, t) = |\tilde{y}(ft)|^2. \quad (12)$$

The switching function  $y(t)$  toggles between  $+1$  and  $-1$  for every applied  $\pi$  pulse between free precession periods. For noise spectroscopy, the overlap between the power spectral density (PSD) and the filter function is then used to evaluate the noise sensitivity [PSD (yellow) and  $|F|$  (black line) in Fig. 1(b)]. This method can also be used to filter out noise

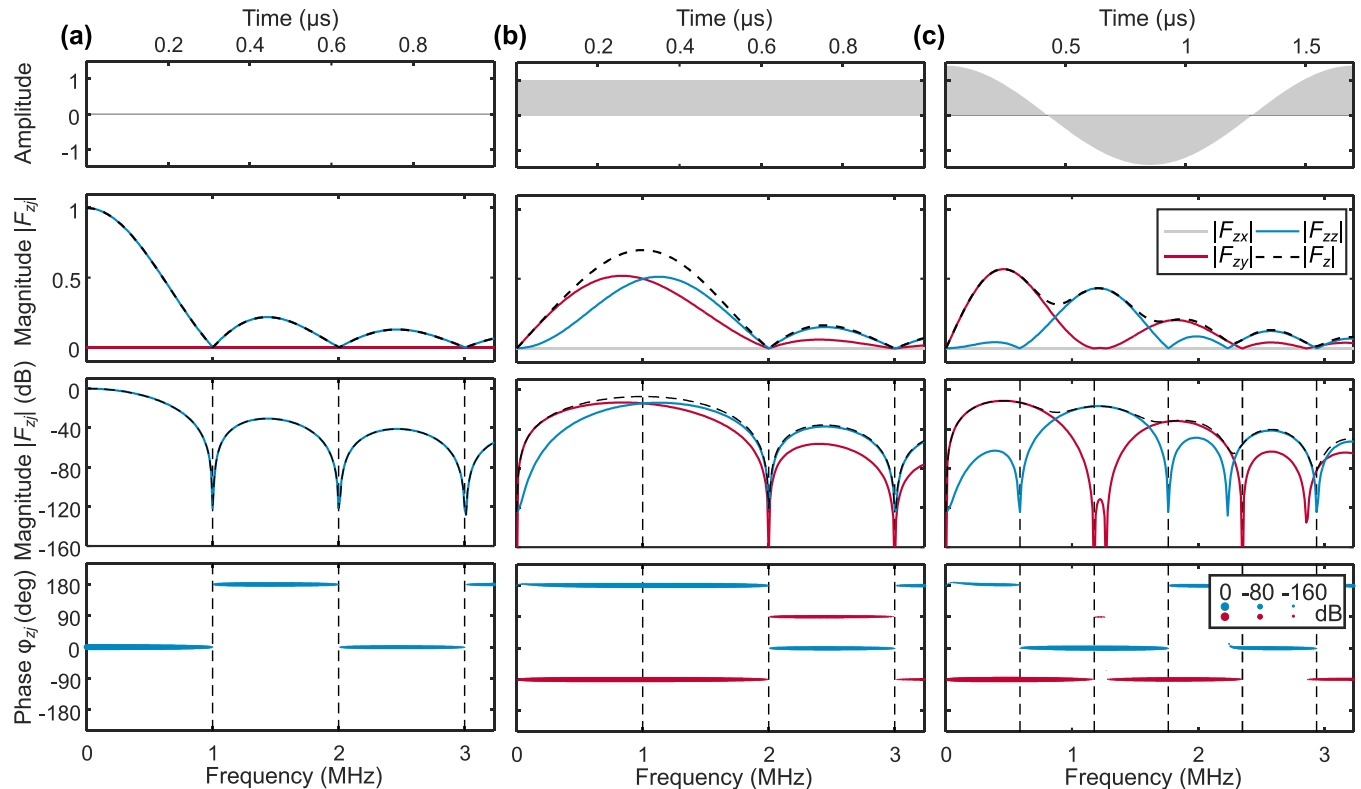


FIG. 2. Examples of the full filter function. Driving field over a time  $T$ , filter function magnitude  $|F_{zj}|$  (unitless and dB), and corresponding perturbation phase  $\phi_{zj}$  as a function of perturbation frequency for (a) a bare system, (b) a dressed system, and (c) a cosine-modulated dressed system. Multiples of  $1/T$  are shown with vertical dashed lines.

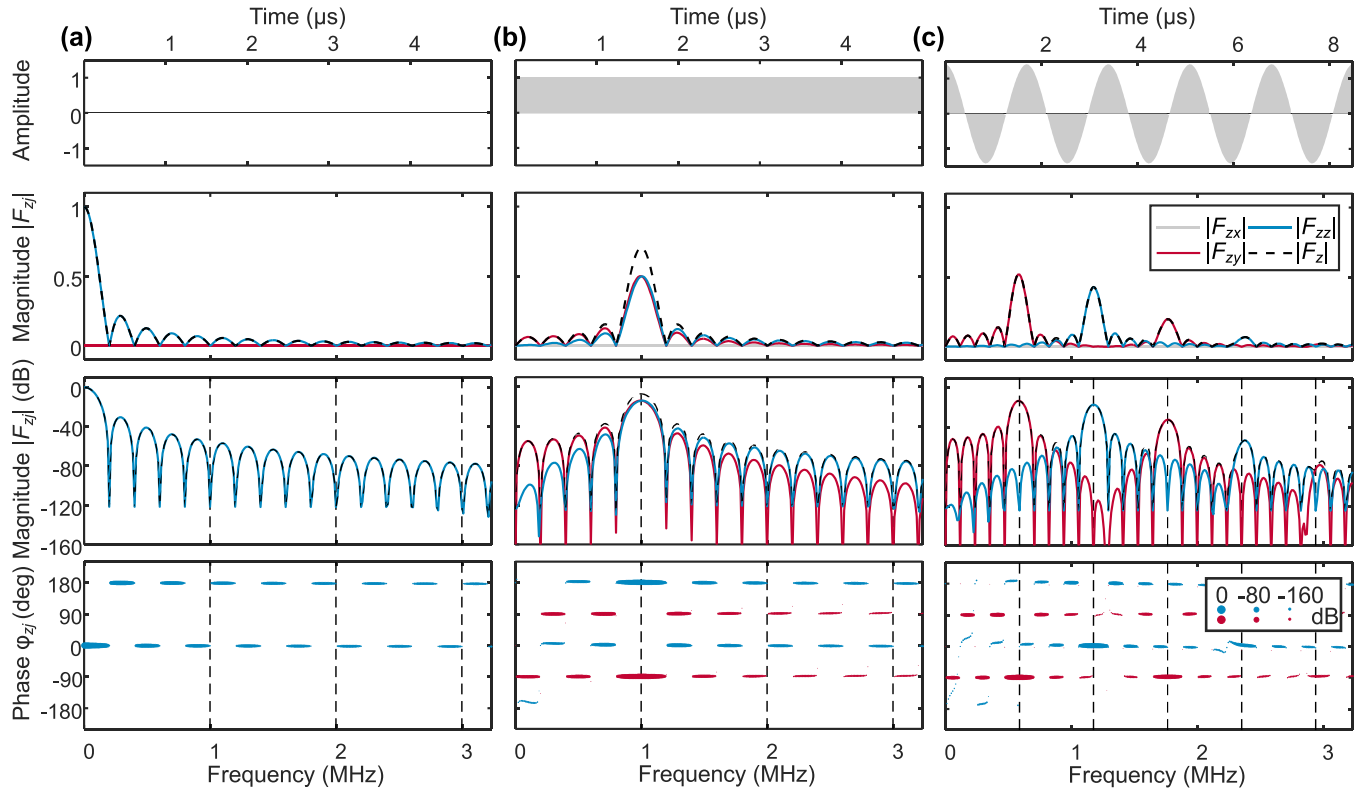


FIG. 3. Multiperiod filter function. The same examples as in Fig. 2 but with a time corresponding to five periods. (a) Bare system, (b) dressed system, and (c) cosine-modulated dressed system.

during control [18,29,30]. However, by calculating the filter function in this simplified way, all directional and phase information is lost.

This work involves the integration of directional and phase information, as well as the application of it to construct single-qubit controls for driven systems. The method developed here merely extracts the parameters to enable control of such systems, whereas previous literature focuses on undriven systems where control is, in principle, trivial, but the aim is to construct control with certain filtering properties as an optimization problem. Expanding this method to multiqubit scenarios is not trivial [31]. One approach is focusing on the error rates to turn it into a signal-processing problem by making use of the sparsity of the dynamics [32]. This can aid in multiqubit control analysis and we leave this for future work.

We study next a few examples to help interpret the full information from the complex filter function. In Fig. 2 the driving fields and filter functions for a bare system, a dressed system, and a modulated dressed system (according to the SMART protocol [19]) are shown. For the dressed example we use an amplitude corresponding to 1-MHz Rabi oscillations, and we use the same power for the modulated dressed example. However, any frequency scale is applicable. Here the three components of the decomposed filter function are shown together with the square root of the sum of squares. The latter represents the simplified version [Eq. (12)]. The magnitude of each component represents the effective rotation around the respective axis and the phase corresponds to the maximum magnitude at any frequency.

The bare system in Fig. 2(a) is sensitive to dc noise with decreasing filter gain for higher frequencies. Low-frequency noise causes rotation around axis  $z$ , which can be seen from the nonzero value of  $|F_{zz}|$  [blue trace (light gray)]. The bare system filter function has zero magnitude at multiples of  $1/T$  (dashed vertical lines), where  $T$  is the total duration. These are the cases where the noise effectively results in an identity gate (e.g.,  $2\pi$  phase accumulation). The bare system can, in fact, not be seen as a perturbation problem, since  $\delta\beta\sigma_z$  is the only term in the Hamiltonian.

The dressed system in Fig. 2(b), on the other hand, is insensitive to dc noise and mainly responds to  $1/T$  as indicated by the  $|F_{zz}|$  and  $|F_{zy}|$  peaks at 1 MHz. This frequency noise causes  $z$  rotation and/or  $y$  rotation depending on the phase of the noise.

The cosine-modulated dressed case in Fig. 2(c) is also insensitive to dc noise, but responds to  $1/T$  and its multiples with decreasing filter gain for increasing frequency. In this case, the peaks of  $|F_{zy}|$  and  $|F_{zz}|$  are separated both in frequency and phase, with corresponding frequencies  $1/T \approx 0.6$  MHz and  $2/T \approx 1.2$  MHz and phases  $-90^\circ$  and  $0^\circ$ . In Fig. 3, the same driving fields are used but with five times longer duration, showing narrower bandwidth of the filter functions.

### III. FROM FILTER FUNCTIONS TO THE GEOMETRIC FORMALISM

The geometric formalism is the particular case of the  $f = 0$  filter function [13]. Here we expand the geometric formalism

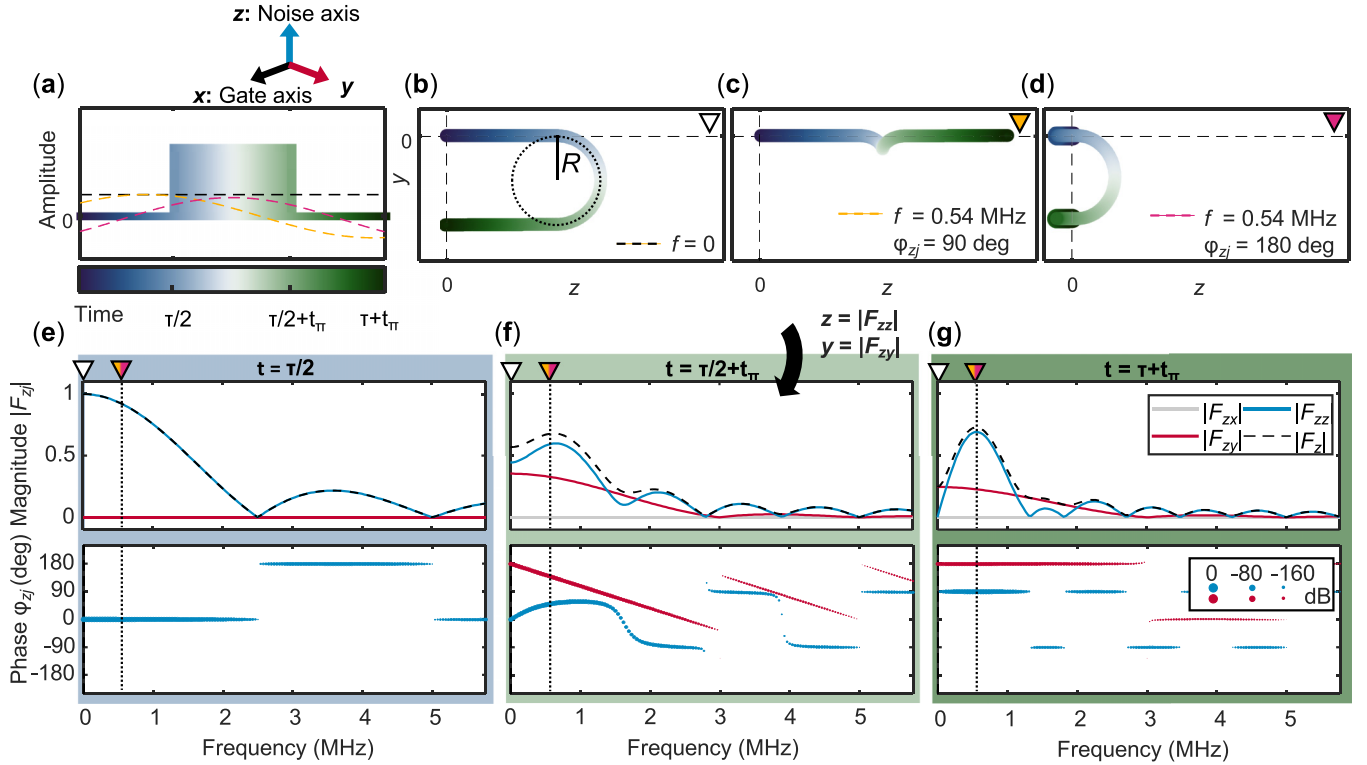


FIG. 4. Noise susceptibility from geometric formalism and filter function. (a) Hahn echo sequence for the  $\pi$  gate on the  $x$  axis with three different noise implementations. [(b)–(d)] The three corresponding geometric space curves. [(e)–(g)] Filter function magnitude  $|F_{zj}|$  and corresponding perturbation phase  $\phi_{zj}$  at three specific time steps. Here,  $\tau/2 = 0.4 \mu\text{s}$  and  $t_\pi = 0.5 \mu\text{s}$ .

to include noise with frequency  $f$  to relate it to the entire filter function. Now we can describe the filter function and the space curve with the same equation [Eq. (6)]. We see in the next example that the filter function is assigned a space curve for each frequency and phase.

We use the example of the Hahn echo sequence to explain the connection between the filter function and the geometric formalism. We use a  $\pi$  pulse on the  $x$  axis with a finite duration, as illustrated in Fig. 4(a), where three different noise frequency cases are considered with space curves in Figs. 4(b)–4(d) and three different times are looked at for the filter function in Figs. 4(e)–4(g) ( $\tau/2$ ,  $\tau/2 + t_\pi$ , and  $\tau + t_\pi$ ). The connection between the filter function components and the 3D space curve in Fig. 4 is given by  $|F_{zz}| = z$ ,  $|F_{zy}| = y$ , and  $|F_{zx}| = x$  for a given time.

For the dc noise case in Fig. 4(b), the system is under free precession for  $t \leq \tau/2$ . This equates to a space curve moving from the origin to an increasing  $z$  value with time. The filter function accumulates a corresponding  $|F_{zz}|$  value [blue trace (light gray) at  $f = 0$  in Fig. 4(e)]. During the  $\pi$  pulse the space curve makes a semicircle in the  $zy$  plane where the radius  $R$  increases with the inverse of the Rabi frequency. This equates to  $|F_{zy}|$  accumulating in Fig. 4(f) [red (dark gray) trace at  $f = 0$ ]. After the final free precession the space curve is back at  $z = 0$ , but now the value of  $y$  is  $2R$ . For the filter function, we see in Fig. 4(g) that  $|F_{zz}|$  is zero, whereas  $|F_{zy}|$  is not [blue and red trace (light and dark gray) at  $f = 0$ , respectively].

For the noise cases with  $f = 0.54$  MHz, the system is under free precession at  $t \leq \tau/2$ , and the space curve moves towards positive or negative  $z$  values depending on the phase

and sign of the noise [Figs. 4(c) and 4(d)]. The  $|F_{zz}|$  filter function magnitude at  $f = 0.54$  MHz in Fig. 4(d) is lower than that for the dc case due to lower noise power. During the  $\pi$  pulse for the case with  $f = 0.54$  MHz and  $\phi_z = 90^\circ$ , the phase shift caused by the  $\pi$  pulse coincides with the change of sign of the noise [Fig. 4(c)]. Therefore, the space curve continues to accumulate the  $z$  value and the  $\pi$ -pulse enhances the noise instead of canceling it out. The case with  $f = 0.54$  MHz and  $\phi_z = 180^\circ$ , on the other hand, makes an approximate semicircle and comes back to  $z = 0$ , but with a finite  $y$  value. From the filter function data in Fig. 4(g) this can be seen from the  $|F_{zz}|$  peak at  $f = 0.54$  MHz when  $\phi_z = 90^\circ$ , and a nonzero  $|F_{zy}|$  values at the same frequency when  $\phi_z = 180^\circ$ .

#### IV. CONTROLLABILITY USING DECOMPOSED FILTER FUNCTIONS

The geometric formalism and the filter function are first of all used to characterize noise performance. However, both can also be used to describe control. In fact, the way the filter function is defined in this work, with well-defined frequency and phase, is more representative of control signals than of stochastic noise. To make the filter function more accurately portray stochastic noise, one can, for example, average it over different phases. We now treat the perturbation  $\delta\beta$  as control (to be applied synchronously with the global driving field). The noise propagator in Eq. (2) can then be seen as a control propagator instead. In other words, coherent noise with defined frequency and phase is equivalent to control pulses.

Controllability for an arbitrary global driving field is found by locating the peaks in the filter function and extracting the frequency and phase. By applying control pulses with these parameters synchronously with the global field, the desired rotation occurs. In the geometric formalism, this corresponds to a space curve ending up somewhere along the axis of rotation. The rotation magnitude is represented by the filter function gain and the displacement from the origin of the space curve.

This gate representation, using the filter function and the geometric formalism, is useful to look at the effective rotation axis for a given driving field as a function of frequency, phase, and duration. Hence, the filter function and the geometric formalism are useful not only for stochastic quasistatic perturbation in the form of noise but also for intentional ac control perturbations. The gate representation differs from the one in Ref. [13] where the control pulse is included in  $H_{\text{drive}}(t)$  and the gate is represented by the orientation of the final tangent vector relative to the initial one.

Finally we show an example of how to use the filter function to find two-axis control of a complicated three-harmonic global driving field [Fig. 5(a)]. This specific driving field provides as high as 6th-order noise cancellation (see the Appendix for more details). The filter function peaks are located at the 2nd and 5th harmonics (vertical dashed lines at  $\sim 1.2$  MHz and  $\sim 3$  MHz) with phase  $0^\circ$  ( $z$ ) and  $-90^\circ$  ( $y$ ), respectively. The controls are also represented using the corresponding space curves in Fig. 5(b). We find that there are several frequency options that enable two-axis control; however, for quantum computation we want fast gates in order to do maximal gate repetitions before decohering and we therefore choose the most efficient gate implementations with higher filter gain. Two-axis control of the two dressed systems in Figs. 3(b) and 3(c) is also found by simply locating the filter function peaks. These have been demonstrated experimentally in Refs. [9,19].

## V. CONCLUSION

In conclusion we have developed a generalized method to extract the local control pulses for systems driven by arbitrary global fields. In designing the global driving field both the qubit noise and control susceptibility and the power spectral density must be kept in mind. This allows for controllable arrays of qubits robust against low-frequency noise throughout the entire computation with control frequencies in strategic bands. The method is also useful for noise analysis including directional and phase information.

## ACKNOWLEDGMENTS

We acknowledge support from the Australian Research Council (Grants No. FL190100167 and No. CE170100012) and the U.S. Army Research Office (Grant No. W911NF-17-1-0198). The views and conclusions contained in this document are those of the authors and should not be interpreted as representing the official policies, either expressed or implied, of the Army Research Office or the U.S. Government. The U.S. Government is authorized to reproduce and distribute reprints for Government purposes notwithstanding

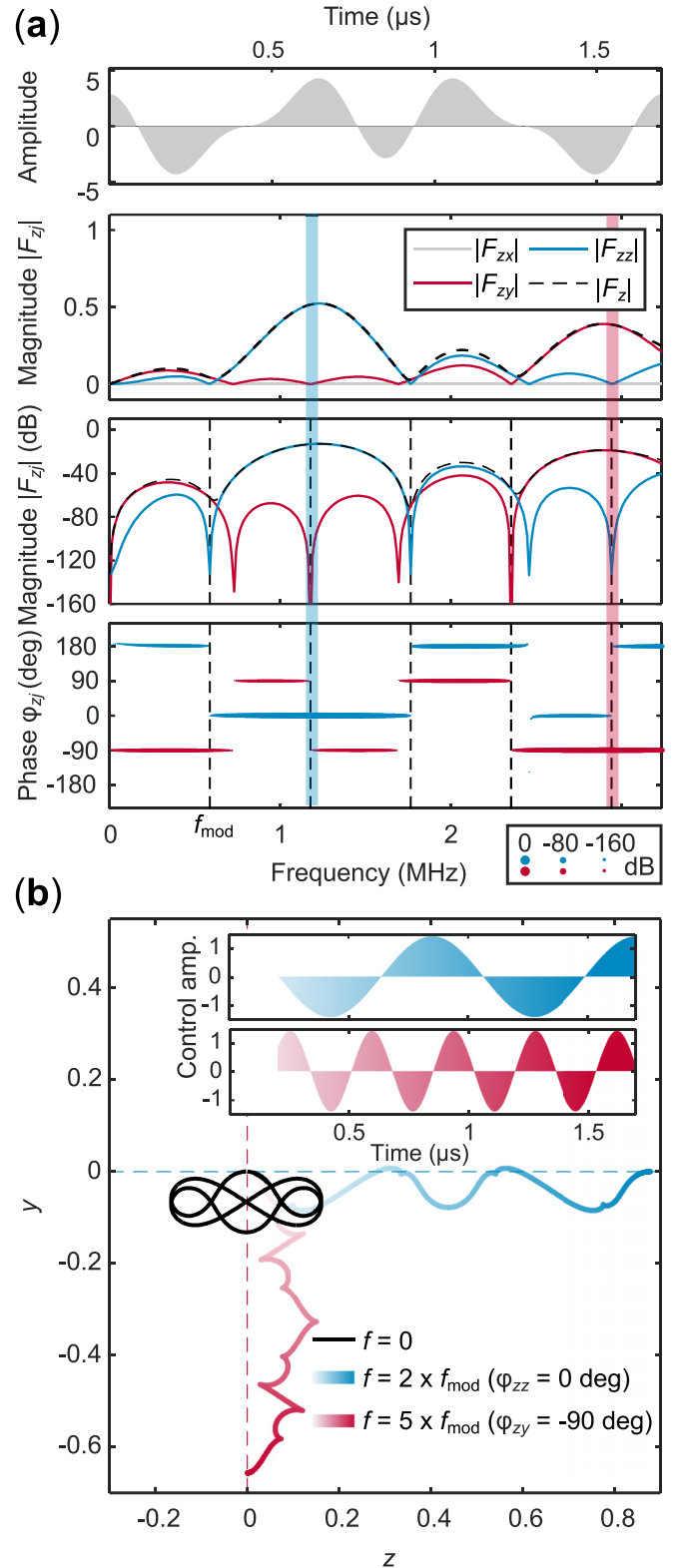


FIG. 5. Gate representation with filter function and geometric formalism. (a) The driving field constructed from the weighted sum of three harmonics and the corresponding filter function  $|F_{zj}|$  and perturbation phase  $\phi_{zj}$ . (b) Controls and space curves. The space curves for three different frequencies are shown. Two-axis controllability ( $z$  rotation and  $y$  rotation) is found with the second and fifth harmonics.

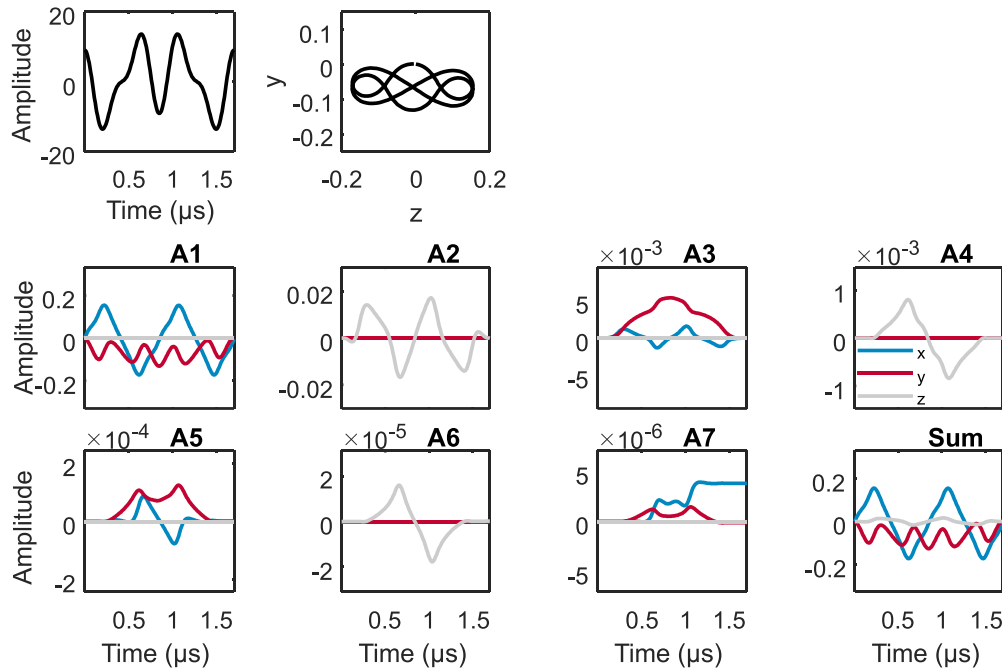


FIG. 6. Higher-order Magnus expansion terms. Driving field, space curve, and higher-order Magnus expansion terms for one period of a driving field consisting of three harmonics with quasistatic noise assumption, showing noise cancellation up to the 6th order. The noise magnitude equals the driving amplitude.

any copyright notation herein. I.H and A.E.S acknowledge support from Sydney Quantum Academy.

#### APPENDIX: HIGHER-ORDER FILTER FUNCTIONS

In Eq. (6) the filter function is calculated using the first term of the Magnus expansion series. However, we can truncate the series at higher order and this will give a more accurate representation of the noise and control susceptibility of the system. Higher-order terms of the Magnus expansion series are calculated with iterative integrals of right-nested commutators [33]. The full Magnus expansion when considering only the  $i$ -axis noise is given by

$$A_i(t) = \delta_i A_{1i}(t) + \delta_i^2 A_{2i}(t) + \delta_i^3 A_{3i}(t) + \dots \quad (\text{A1})$$

Using the gradient ascent pulse engineering (GRAPE) algorithm, we find that by combining three harmonics for the

driving field we are able to cancel out quasistatic noise up to the sixth order. The parameters for the driving field are given here as

$$H(t) = \Omega(h_1 \cos(2\pi ft) + h_2 \cos(6\pi ft) + h_3 \cos(10\pi ft)), \quad (\text{A2})$$

$$\begin{aligned} h_1 &= \cos(\gamma) \cos(\delta), \\ h_2 &= \cos(\gamma) \sin(\delta), \\ h_3 &= \sin(\gamma), \end{aligned} \quad (\text{A3})$$

with  $\Omega = -2.57453$ ,  $\gamma = -0.49001$ , and  $\delta = -1.04785$ . The seven first terms of the three-harmonic drive for quasistatic noise are shown in Fig. 6, where the magnitude of the higher-order terms are seen to decrease exponentially. This can be seen from the sum which closely resembles the first term. The first nonzero term represents the  $T_1$  axis of the driven system, in this case  $\sigma_x$ .

- 
- [1] A. Saraiva, W. H. Lim, C. H. Yang, C. C. Escott, A. Laucht, and A. S. Dzurak, *Adv. Funct. Mater.* **32**, 2105488 (2022).
- [2] K. W. Chan, W. Huang, C. H. Yang, J. C. C. Hwang, B. Hensen, T. Tanttu, F. E. Hudson, K. M. Itoh, A. Laucht, A. Morello, and A. S. Dzurak, *Phys. Rev. Appl.* **10**, 044017 (2018).
- [3] K. M. Itoh and H. Watanabe, *MRS Commun.* **4**, 143 (2014).
- [4] C. H. Yang, K. W. Chan, R. Harper, W. Huang, T. Evans, J. C. C. Hwang, B. Hensen, A. Laucht, T. Tanttu, F. E. Hudson, S. T. Flammia, K. M. Itoh, A. Morello, S. D. Bartlett, and A. S. Dzurak, *Nat. Electron.* **2**, 151 (2019).
- [5] A. Vepsäläinen, R. Winik, A. H. Karamlou, J. Braumüller, A. D. Paolo, Y. Sung, B. Kannan, M. Kjaergaard, D. K. Kim, A. J. Melville, B. M. Niedzielski, J. L. Yoder, S. Gustavsson, and W. D. Oliver, *Nat. Commun.* **13**, 1932 (2022).
- [6] S. G. J. Philips, M. T. Madzik, S. V. Amitonov, S. L. de Snoo, M. Russ, N. Kalhor, C. Volk, W. I. L. Lawrie, D. Brousse, L. Tryputen, B. P. Wuetz, A. Sammak, M. Veldhorst, G. Scappucci, and L. M. K. Vandersypen, *Nature (London)* **609**, 919 (2022).
- [7] E. Paladino, Y. M. Galperin, G. Falci, and B. L. Altshuler, *Rev. Mod. Phys.* **86**, 361 (2014).
- [8] M. Baur, S. Filipp, R. Bianchetti, J. M. Fink, M. Göppl, L. Steffen, P. J. Leek, A. Blais, and A. Wallraff, *Phys. Rev. Lett.* **102**, 243602 (2009).

- [9] A. Laucht, R. Kalra, S. Simmons, J. P. Dehollain, J. T. Muhonen, F. A. Mohiyaddin, S. Freer, F. E. Hudson, K. M. Itoh, D. N. Jamieson, J. C. McCallum, A. S. Dzurak, and A. Morello, *Nat. Nanotechnol.* **12**, 61 (2017).
- [10] A. E. Seedhouse, I. Hansen, A. Laucht, C. H. Yang, A. S. Dzurak, and A. Saraiva, *Phys. Rev. B* **104**, 235411 (2021).
- [11] I. Hansen, A. E. Seedhouse, A. Saraiva, A. Laucht, A. S. Dzurak, and C. H. Yang, *Phys. Rev. A* **104**, 062415 (2021).
- [12] B. E. Kane, *Nature (London)* **393**, 133 (1998).
- [13] J. Zeng, C. H. Yang, A. S. Dzurak, and E. Barnes, *Phys. Rev. A* **99**, 052321 (2019).
- [14] E. Barnes, F. A. Calderon-Vargas, W. Dong, B. Li, J. Zeng, and F. Zhuang, *Quantum Sci. Technol.* **7**, 023001 (2022).
- [15] T. J. Green, J. Sastrawan, H. Uys, and M. J. Biercuk, *New J. Phys.* **15**, 095004 (2013).
- [16] T. Hangleiter, P. Cerfontaine, and H. Bluhm, *Phys. Rev. Res.* **3**, 043047 (2021).
- [17] P. Cerfontaine, T. Hangleiter, and H. Bluhm, *Phys. Rev. Lett.* **127**, 170403 (2021).
- [18] G. A. Paz-Silva and L. Viola, *Phys. Rev. Lett.* **113**, 250501 (2014).
- [19] I. Hansen, A. E. Seedhouse, K. W. Chan, F. E. Hudson, K. M. Itoh, A. Laucht, A. Saraiva, C. H. Yang, and A. S. Dzurak, *Appl. Phys. Rev.* **9**, 031409 (2022).
- [20] M. A. Nielsen and I. L. Chuang, *Quantum Computation and Quantum Information* (Cambridge University, Cambridge, England, 2000).
- [21] M. J. Biercuk, H. Uys, A. P. VanDevender, N. Shiga, W. M. Itano, and J. J. Bollinger, *Nature (London)* **458**, 996 (2009).
- [22] M. J. Biercuk, A. C. Doherty, and H. Uys, *J. Phys. B: At. Mol. Opt. Phys.* **44**, 154002 (2011).
- [23] V. M. Frey, S. Mavadia, L. M. Norris, W. de Ferranti, D. Lucarelli, L. Viola, and M. J. Biercuk, *Nat. Commun.* **8**, 2189 (2017).
- [24] A. G. Kofman and G. Kurizki, *Phys. Rev. Lett.* **87**, 270405 (2001).
- [25] A. G. Kofman and G. Kurizki, *Phys. Rev. Lett.* **93**, 130406 (2004).
- [26] R. K. L. Colmenar and J. P. Kestner, *Phys. Rev. A* **106**, 032611 (2022).
- [27] Ł. Cywiński, R. M. Lutchyn, C. P. Nave, and S. Das Sarma, *Phys. Rev. B* **77**, 174509 (2008).
- [28] J. M. Martinis, S. Nam, J. Aumentado, K. M. Lang, and C. Urbina, *Phys. Rev. B* **67**, 094510 (2003).
- [29] A. Soare, H. Ball, D. Hayes, J. Sastrawan, M. C. Jarratt, J. J. McLoughlin, X. Zhen, T. J. Green, and M. J. Biercuk, *Nat. Phys.* **10**, 825 (2014).
- [30] F. K. Malinowski, F. Martins, P. D. Nissen, E. Barnes, Ł. Cywiński, M. S. Rudner, S. Fallahi, G. C. Gardner, M. J. Manfra, C. M. Marcus, and F. Kuemmeth, *Nat. Nanotechnol.* **12**, 16 (2017).
- [31] D. Buterakos, S. Das Sarma, and E. Barnes, *PRX Quantum* **2**, 010341 (2021).
- [32] M. Rimbach-Russ, S. G. J. Philips, X. Xue, and L. M. K. Vandersypen, *arXiv:2211.16241*.
- [33] A. Arnal, F. Casas, and C. Chiralt, *J. Phys. Commun.* **2**, 035024 (2018).